Neutron scattering and susceptibility measurements on single crystals of $Cu_{1-x}(Zn/Ni)_xGeO_3$

1996 J. Phys.: Condens. Matter 8 6251

(http://iopscience.iop.org/0953-8984/8/34/014)

J. Phys.: Condens. Matter **8** (1996) 6251–6266. Printed in the UK

Neutron scattering and susceptibility measurements on single crystals of $Cu_{1-x}(Zn/Ni)_xGeO_3$

S Coad†, J-G Lussier‡, D F McMorrow‡ and D McK Paul†

† Department of Physics, University of Warwick, Coventry CV4 7AL, UK

‡ Department of Solid State Physics, Risø National Laboratory, DK-4000 Roskilde, Denmark

Received 10 June 1996

Abstract. Single-crystal derivatives of the spin–Peierls (S–P) system, $CuGeO_3$, doped with Zn (0.5 to 2.4%) and Ni (1.7 to 6%) have been studied using SQUID magnetometry and neutron scattering. Our study shows that the impurities act to suppress the S–P state and produce a 3D Néel state at low temperatures. A phase diagram is constructed which shows that doping with either Zn ($S = 0$) or Ni ($S = 1$) leads to qualitatively similar results: the temperature at which the transition to the S–P state occurs decreases linearly with dopant concentration, whereas the Néel temperature, T_N, initially increases to a maximum at around 4% and then decreases for higher concentrations. These results are discussed with reference to models of defects in 1D spin chains and to earlier experimental work on this system. One difference between the Zn- and Ni-doped samples is that in the Néel state the Cu^{2+} moments in the former point along the c-axis, while in the latter they are along the a-axis.

1. Introduction

The inorganic 1D antiferromagnetic compound, $CuGeO_3$, has received much attention since the discovery in 1993 that it undergoes a spin–Peierls (S–P) transition [1]. In general, quantum Heisenberg antiferromagnetic 1D chains with integer spin values display a Haldane gap [2, 3]. For a Heisenberg antiferromagnetic 1D chain with $S = 1/2$, quantum fluctuations can result in a reduction of the magnetic energy by dimerization of the lattice along the chain, provided the crystal structure can be easily distorted. Then the resulting alternation of exchange coefficients between adjacent sites leads to the creation of a non-magnetic singlet ground state that is separated from the first excited triplet states by a S–P energy gap. In $CuGeO_3$, the S–P transition was first observed from magnetic susceptibility measurements which showed an isotropic exponential decrease below $T_{sp} = 14$ K [1]. Many subsequent measurements have revealed the presence of an energy gap [4, 5]; the triplet nature of the first excited state [6]; and structural dimerization [7], observed through the presence of superlattice Bragg reflections in the wavevector direction $(1/2, k, 1/2)$.Thus the occurrence of a S–P transition in $CuGeO_3$ has been clearly established.

The orthorhombic structure of $CuGeO_3$ is composed of linear chains of strongly coupled Cu^{2+} ions along the c-axis, well separated from each other by Ge–O chains, as shown in figure 1. Measurement of exchange coefficients along each axis direction confirm the 1D nature of this compound,($J_b/J_c \approx 0.1$, $J_a/J_c \approx 0.011$) [4] although there is a significant interchain interaction, especially along the b-axis. In contrast to organic S–P compounds such as TTF-$CuS_4C_4(CF_3)_4$, TTF-$AuS_4C_4(CF_3)_4$ and (MEM)-$(TCNQ)_2$ [8, 9, 10], which have magnetic moments that arise from unpaired electrons in covalent π-bonds, $CuGeO_3$ has

0953-8984/96/346251+16$19.50

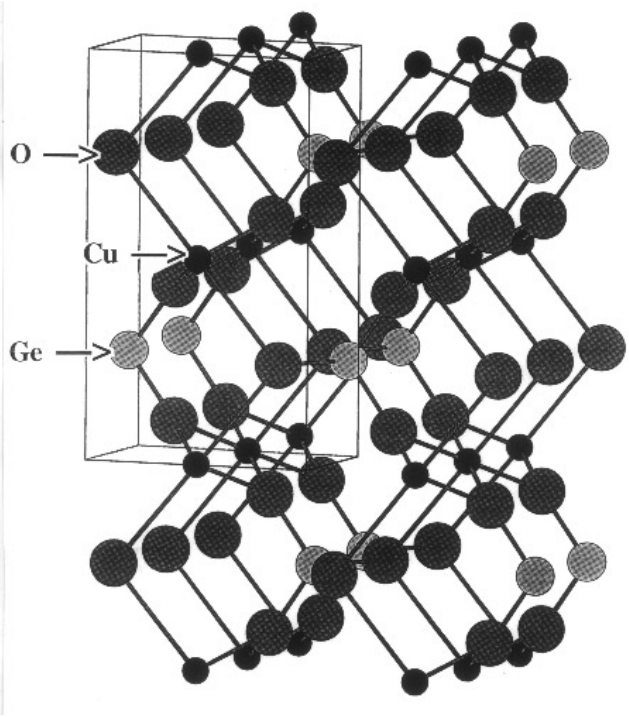

Figure 1. The crystal structure of $CuGeO_3$ viewed along the *c*-axis with the *a*-axis horizontal and the *b*-axis vertical. The Cu^{2+} ions are the small black circles, while the medium light circles are the Ge^{4+} and the large dark circles correspond to the O^{2-} ions. The box delineates the unit cell at room temperature.

localized spins on the Cu^{2+} ions that couple through a superexchange interaction along the *c*-axis. As was realized at an early stage, $CuGeO_3$ is an ideal compound for studying the effect of doping on the S–P ground state. Initial studies by Hase *et al* [1] have shown that $CuGeO_3$ is particularly susceptible to the introduction of impurities: only a few % is sufficient to suppress the S–P ground state and to drive the system eventually into a different magnetic phase at low temperature. Thus the study of high-quality doped crystals with precisely determined composition is required for a greater understanding of the mechanism underlying the S–P transition. Until recently, the nature of the low-temperature magnetic phase was a matter of some controversy as several studies [11, 12] claimed to observe a spin-glass phase that might arise from the freezing of unpaired chains in the vicinity of the impurity. Many investigations have been made on crystals of $CuGeO_3$ with different substitutions for either the Cu^{2+} ions (Zn^{2+}, Ni^{2+}, Mg^{2+}) or the Ge^{4+} ions (Si^{4+}) [13, 14, 15]. What is remarkable is that all report the appearance of a 3D antiferromagnetic state at low temperature, qualitatively independent of spin and dopant.

In this paper we concentrate on the effect of doping Zn and Ni impurity ions into $CuGeO_3$, namely the suppression of the S–P transition and the appearance of a 3D magnetic phase at low temperature. We have chosen to study a series of single crystals of $CuGeO_3$ doped with a range of concentrations of Zn^{2+} ($S = 0$) or Ni^{2+} ($S = 1$). The radii of these impurity ions are closest to that of Cu^{2+} and therefore they distort the crystal structure minimally. This paper is organized as follows. The method of crystal growth is described in

Table 1. Crystals of $Cu_{1-x}A_xGeO_3$ (A = Zn, Ni) grown by the floating-zone method in an infra-red image furnace. The % dopant concentration given in the first column was determined by averaging the concentration obtained from mass spectroscopy measurements (with an accuracy of ppm) on segments taken from each end of the crystal. The third column represents the variation in dopant concentration across the crystal.

	Crystal	Dimensions ($a \times b \times c$) (mm^3)	Dopant concentration range (%)
Pure	$CuGeO_3$	$2 \times 4 \times 32$	<1 ppm
Zn-doped	1.2	$2 \times 3 \times 39$	0.09
(%)	1.5	$2 \times 3 \times 32$	0.18
	2.0	$2 \times 4 \times 31$	0.36
	2.4	$2 \times 3.5 \times 32$	0.27
Ni-doped	1.7	$2 \times 3 \times 32$	0.07
(%)	1.9	$2 \times 3.5 \times 37$	0.12
	2.9	$2 \times 3 \times 35$	0.04
	3.3	$2 \times 3 \times 31$	0.38
	6.0	$5 \times 4 \times 21$	0.24

section 2, and then susceptibility data and analysis are presented in section 3.1. Our neutron scattering results are given in section 3.2 and focus on the variation of order parameters with temperature at the structural superlattice position (1/2, 3, 1/2); the appearance of long-range AF order; and the variation of T_N with dopant concentration; the observation of magnetic saturation in a 2.4% Zn-doped crystal; and evidence that the magnetic moment direction in the Néel state changes from c^* to a^* when the crystal is doped with Ni instead of with Zn. Analysis and discussion follows in section 4 and our overall conclusions are given in section 5. A short report on some of these data has been published previously [16].

2. Experimental details

The single crystals studied were grown by the floating-zone method in 1 atm of flowing oxygen. Seed crystals were used to initiate growth along the c-axis, at a slow rate of 2 mm h^{-1}, thus ensuring a regular deposition of crystal layers and good sample quality. Laue x-ray diffraction photographs and the presence of visible a^* cleavage planes, confirmed that the samples were single crystals. The composition and dimensions of the crystals used (after removal of sections for susceptibility measurements) are listed in table 1. All of the crystals were grown in a single pass through the floating zone and were not subsequently annealed.

Since the value of T_{sp} is known from early studies to be concentration dependent [17] and the crystals are relatively large, special care was taken to ensure homogeneity in composition along the entire length of the crystals. Small pieces from the ends of each crystal were dissolved and analysed using an inductively coupled plasma mass spectrometer to measure the ratio of $^{58}Ni/^{65}Cu$ or $^{66}Zn/^{65}Cu$ with accuracy of the order of 1 ppm. We found considerable differences between nominal and actual concentrations; for instance the most highly doped crystal—nominally 10% Ni^{2+} doped—was in fact only 6% Ni^{2+} doped. However, there is no substantial concentration gradient over the entire length of any of the samples, as can be seen from the third column in table 1.

3. Results

3.1. Susceptibility

The sections removed from the end of each single crystal had susceptibility measurements taken using a SQUID (Quantum Design, USA) magnetometer over the temperature range of 2 K to 300 K. Magnetization was recorded in an applied field of 0.01 T with the c-axis of the crystal perpendicular or parallel to the field. Although the S–P transition is second order, and therefore should not exhibit hysteresis, care was taken to ensure that the samples were cooled in nominally zero field. We first present results on the pure compound.

$CuGeO_3$ has two main regions for susceptibility data (above and below T_{sp}). A fit to each part can help determine the nature of the coupling within each spin chain along c (intrachain) and the degree of interaction between them (interchain). The high-temperature susceptibility of a 1D antiferromagnet is usually an effective way to measure the magnitude of the exchange interaction, J. In the case of undoped $CuGeO_3$ the value of J determined depends on the model used. The following review compares our data with previous results.

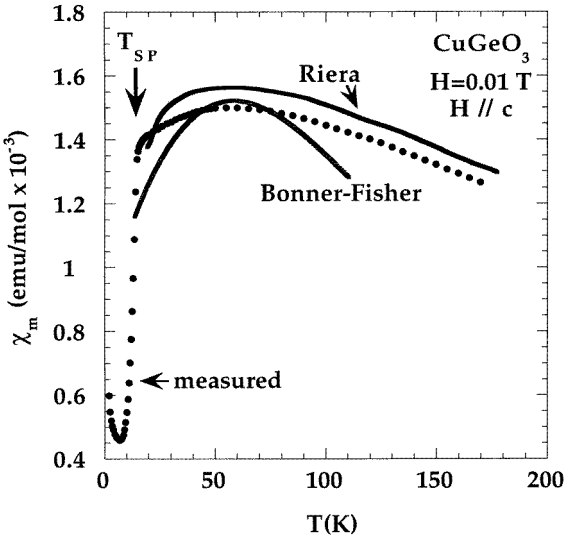

Figure 2. High-temperature magnetic susceptibility of a section of $CuGeO_3$ measured with $\boldsymbol{H}$ parallel to c. Two theoretical curves are included for comparison. The Bonner–Fisher model describes a uniform Heisenberg interaction along the spin chains by extrapolating chains of magnetic moments [18]; the curve labelled Riera corresponds to a Heisenberg model that includes next-nearest-neighbour interactions along the chain also [23].

Figure 2 shows the high-temperature dc susceptibility data for $CuGeO_3$ aligned with the c-axis parallel to a field of 0.01 T, compared with two theoretical predictions for an infinite-chain ($S = 1/2$) Heisenberg antiferromagnet. The Bonner and Fisher curve [18] describes a uniform Heisenberg interaction along the spin chains in the absence of dimerization. The curve is produced via a numerical method that takes regular finite chains of N magnetic moments and extrapolates to $N \to \infty$ and $T \to 0$. While experimental results and the Bonner–Fisher model fit well for the organic S–P compounds [20], the shape of the curve is not sufficiently similar to the measured data for $CuGeO_3$ to allow the quasi-1D magnetic state above T_{sp} to be identified as solely 1D Heisenberg antiferromagnetism. Introduction

of the anisotropy parameter γ into the Heisenberg–Ising Hamiltonian [18] permits a small amount of interchain coupling but does not greatly improve the fit. Nevertheless, a value of the exchange parameter J can be obtained by matching the broad maximum at 53 K in the susceptibility data to the maximum in the Bonner–Fisher curve. We have reproduced Hase's result [1] with $J = 88$ K. An alternative method was used by Nishi *et al* [4] and Regnault *et al* [14] who found $J = 120$ K from inelastic neutron measurements of the dispersions (below T_{sp}) and then applied the des Cloizeaux and Pearson formula for the characteristic energy of a 1D excitation [21]. However, the latter method does not describe a S–P system near the antiferromagnetic zone centre and does not lead to the reported value of 1.93 meV for the S–P gap. A recent ultrahigh-field measurement employing electromagnetic flux compression to reach fields of up to 500 T produced a value for the coupling constant of $J = 183$ K [22].

Other formulations based on an ($S = 1/2$) Heisenberg model with both nearest-neighbour and next-nearest-neighbour antiferromagnetic interactions have recently been proposed. This is justified in $CuGeO_3$ due to the presence of the non-linear Cu–O–O–Cu superexchange paths. Riera and Dobry [23] have presented a model with $J = 160$ K in the absence of dimerization by setting $\alpha = 0.36$, where α is the ratio between nearest- and next-nearest-neighbour exchange coefficients. Then a reasonable fit to the shape of the maximum of the susceptibility is obtained. However, as this value of α is greater than a critical value $\alpha_c = 0.24$ obtained using the Heisenberg formulation, this model predicts the presence of a small spin gap even when $T > T_{sp}$. As yet there is no conclusive proof of the existence of such a gap above T_{sp}. Castilla *et al* [24] forced α to equal α_c in order to avoid the complications of a spin gap but sacrificed the agreement with the susceptibility data, obtaining a value of $J = 150$ K. Yet another alternative is to introduce 2D interchain coupling as well as second-neighbour interactions. If this is done, α_c is not restricted within the Heisenberg model but can change its value. In the short-correlation limit, such as for a spin-ladder system where interchain coupling extends solely to the neighbouring chains, the predicted excitation spectra show a spin gap above T_{sp} with the value of α_c expected to be lower than 0.24. On the other hand, when long-range 2D intrachain order occurs, the excitation is gapless and compensated with a larger value of α_c. Therefore it is possible that relatively long-range interchain interactions in $CuGeO_3$ can modify the value of α_c to 0.36 or above. Overall there is little agreement on the value of J which has made it difficult to establish that the excitations from a S–P state are different from those of an antiferromagnet [25].

Low-temperature susceptibility measurements of $CuGeO_3$ are also useful for examining the S–P transition which is characterized by an exponential decrease below T_{sp}. Susceptibility measurements of $CuGeO_3$ below 20 K are depicted in figure 3 and are fitted with the equation

$$\chi(T) = \frac{a}{T} + \frac{b}{T}\mathrm{e}^{-c/T}. \tag{1}$$

Here a, b and c are constants and the exponential term arises from the Bulaevskii mean-field model [20] for a 1D magnetic system coupled to a 3D phonon field; and the $1/T$ term models the observed increase at low temperatures. While this low-temperature rise in susceptibility has often been dismissed as a consequence of magnetic impurities, our sample of $CuGeO_3$ contains <1 ppm of other magnetic ions. Instead, the low-T divergence may be plausibly explained using the arguments of Liu *et al* [27] who describe the susceptibility of two suspected S–P compounds, (6MAP)$CuCl_3$ and (3MAP)$CuCl_3$. While paramagnetic impurities in our crystals are unlikely, another possibility is broken-chain effects arising from imperfections in the crystal lattice that produce a statistical variation in chain length.

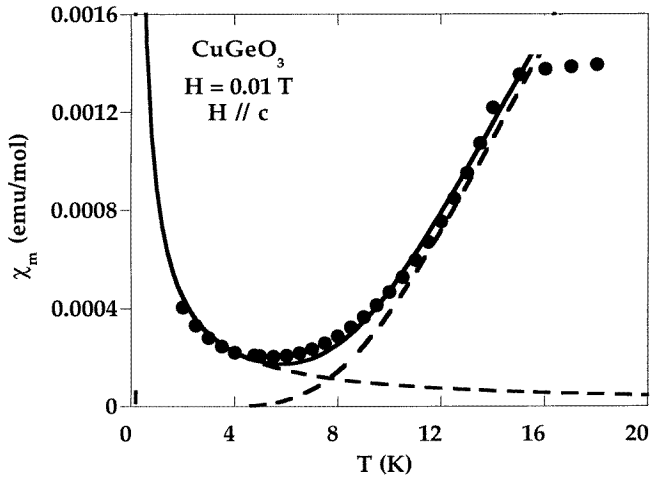

Figure 3. Low-temperature susceptibility for $CuGeO_3$ in a field of 0.01 T fitted with an exponential curve and a $1/T$ function to model the low-T upward turn.

In the 1D Heisenberg AF model, chains with an odd number of spins produce a χ that diverges as $1/T$ as $T \rightarrow 0$.

Susceptibility curves for $CuGeO_3$ are compared to those of $Cu_{1-x}Zn_xGeO_3$ and $Cu_{1-x}Ni_xGeO_3$ for a range of x, in figure 4. The data are normalized to 1 above T_{sp} to emphasize the characteristic features such as the suppression of T_{sp} as the dopant concentration increases. Qualitatively our measurements have the same shape as those of Hase *et al* [12] and Ajiro *et al* [28] who have performed extensive measurements on a range of Ni- and Zn-doped crystals of $CuGeO_3$. Our susceptibility data were partly taken as a means of characterizing the samples for later neutron scattering work which allows the nature of each transition to be determined.

From the graphs in figure 4 it is clear that the transition to the S–P state is suppressed with increasing dopant concentration; that there is still a $1/T$ low-temperature rise; and that another transition is visible in the 1.5% and 2% Zn-doped crystals which exhibit cusps at $\approx$4 K.

Figure 5 shows susceptibility measurements on a 2.4% Zn-doped crystal with a field of 0.01 T perpendicular and parallel to the c-axis of the crystal section. $\chi \rightarrow 0$ when H is directed along the spin direction; therefore from this plot we can say that the Cu^{2+} moments in Zn-doped $CuGeO_3$ lie primarily along the c-axis, whereas the absence of any cusp or decrease in susceptibility in the Ni-doped compounds shown in figure 4, bottom panel, suggests that now the Cu^{2+} moments are aligned in a different direction.

Previous measurements [12, 11] using susceptibility and later muon spin resonance erroneously concluded that this transition was to a spin-glass phase. Our neutron scattering results in the next section clearly demonstrate the transition is to a 3D Néel state.

3.2. Neutron scattering

Elastic neutron scattering experiments were performed on a series of $Cu_{1-x}A_xGeO_3$ (A = Ni, Zn) crystals which had been previously characterized by susceptibility measurements. There were three main objectives: to look at the effect of doping on the S–P transition;

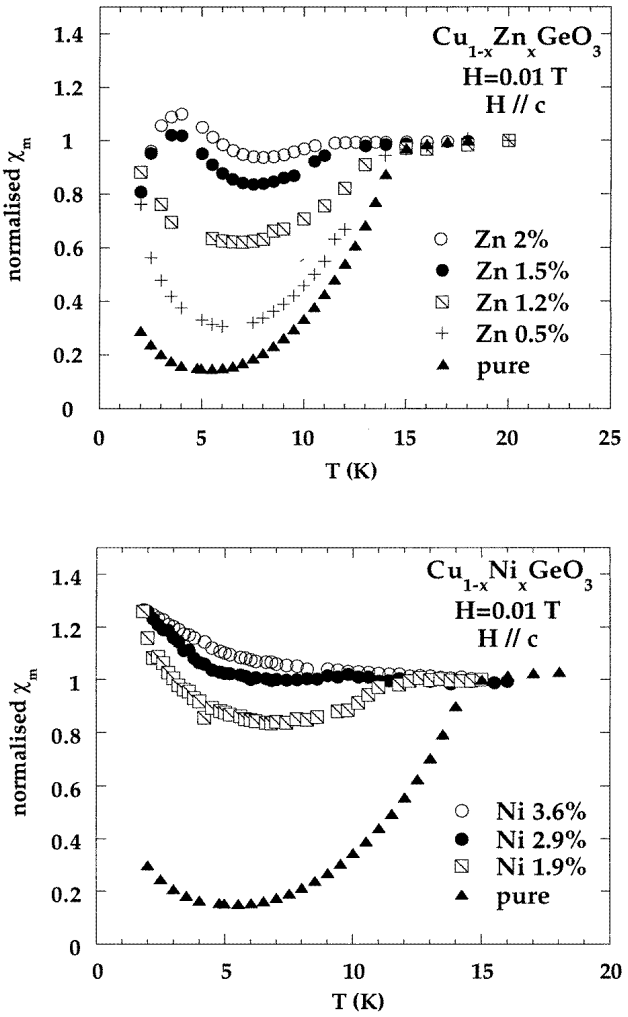

Figure 4. Susceptibility of Zn- and Ni-doped crystals of $CuGeO_3$ for $H = 0.01$ T. The curves were normalized to the values at 20 K and 15 K respectively. The c-axis is parallel to the applied field of 0.01 T.

to characterize the nature of the low-temperature transition in the doped compounds; and to determine the direction of the coupled moments in this low-temperature phase. The experimental results are presented below.

Several neutron scattering experiments were performed on the cold source of the DR3 reactor at Risø National Laboratory using the TAS VI and TAS VII triple-axis spectrometers with incident energy of 4.95 meV or 14.56 meV (reactor-to-detector collimation 30–open–60–120 for both). Measurements were made with the appropriate Be or PG filters in order to eliminate $\lambda/2$ contamination. A helium-flow cryostat was used over the temperature range 1.5 K to 30 K and a pumped ^{3}He refrigerator for the range 0.3 K to 6 K. The crystals were mounted in two different scattering geometries depending on the type of measurement. Magnetic peaks were measured in the $(0, k, l)$ plane and structural superlattice peaks were

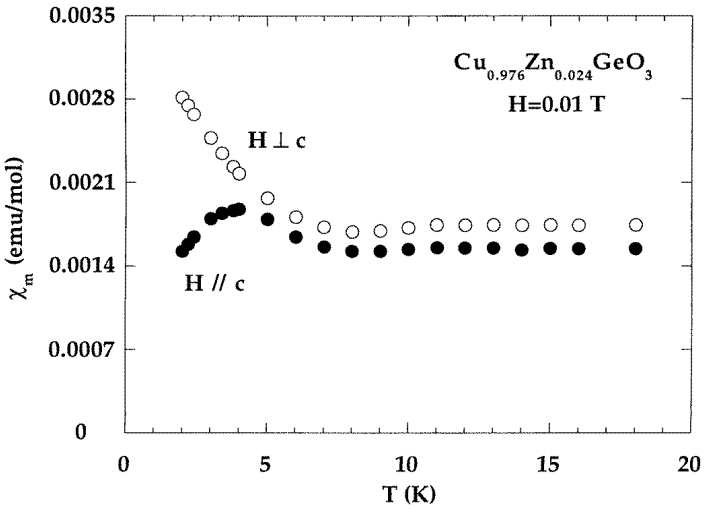

Figure 5. Susceptibility for two different field orientations, $\boldsymbol{H} \parallel \boldsymbol{c}$ and $\boldsymbol{H} \perp \boldsymbol{c}$ in 2.4% Zn-doped $CuGeO_3$. The cusp at the antiferromagnetic transition at 4.5 K shows the overall spin direction to be along the c-axis.

measured in the (h, k, h) plane established by earlier measurements [7]. All of the data shown here have been fitted with Gaussian lineshapes. Before describing the results, we comment on the large discrepancy in intensity observed at the $(0, 2, 0)$ nuclear reflection in each scattering plane. In going from the $(0, k, l)$ to the (h, k, h) scattering plane (a 30-degree rotation of the crystal), the intensity of the $(0, 2, 0)$ reflection increased by a factor of 10. This motion corresponds to a Reninger scan around the scattering wavevector. We suspect that multiple scattering is the explanation, possibly enhanced by the size and shape of the crystal. Therefore normalization of the magnetic scattering to nuclear peaks was rejected and normalization to crystal volume was used instead.

One crucial and determining characteristic of the S–P transition is the appearance of extra superlattice peaks below T_{sp}. These peaks arise from lattice dimerization that is not directly along the Cu^{2+} chain axis but is directed along the $(h + 1/2, k, h + 1/2)$ wavevector [7]. Figures 6(a) and 6(b) show the variation of the order parameter with temperature for a selection of Zn^{2+}- and Ni^{2+}-doped crystals at the superlattice peak position $\boldsymbol{Q} = (1/2, 3, 1/2)$, together with power-law fits near T_{sp}. Values of the order parameter critical exponent (β), obtained from these fits, are listed in table 2 as well as the transition temperatures T_{sp} for each crystal. We do not wish to put undue emphasis on these exponents as their magnitudes depend greatly on the temperature range used for fitting, but we note that at low concentrations they are consistent with Heisenberg theory [29], whereas for higher doping concentrations they approach $\beta = 0.5$ which suggests a mean-field model. Clearly as the dopant concentration increases, T_{sp} diminishes, but the most dramatic effect is the rapid decrease in intensity of the superlattice peaks.

A second characteristic of these doped crystals of $CuGeO_3$ is a low-temperature phase transition, which could be observed as a cusp in the susceptibility data for the more highly Zn-doped crystals. Our elastic neutron scattering measurements show extra magnetic peaks at the positions $\boldsymbol{Q} = (0, 1, 1/2)$, $(0, 3, 1/2)$, $(0, 1, 3/2)$ and $(0, 3, 3/2)$. Comparison of the widths of rocking curves at magnetic and nuclear peaks demonstrate that long-range

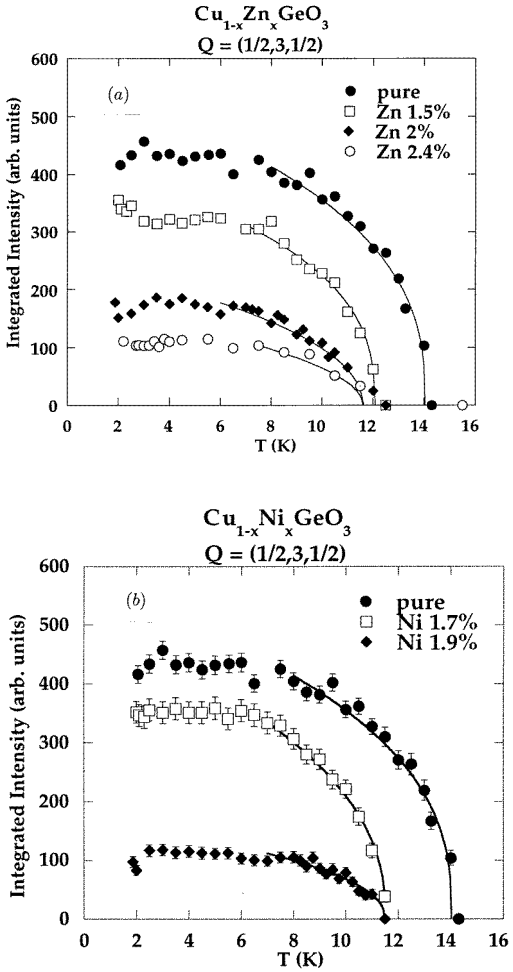

Figure 6. Order parameters at the structural superlattice reflection $\boldsymbol{Q} = (1/2, 3, 1/2)$ for (*a*) three Zn-doped and (*b*) two Ni-doped $CuGeO_3$ crystals with pure $CuGeO_3$ included for comparison. The integrated intensities have been normalized to sample volumes.

antiferromagnetic order exists below the Néel transition temperature, T_N. We have measured the variation of the magnetic order parameter (β_m) at $(0, 1, 1/2)$ with temperature for the ten Zn- and Ni-substituted single crystals listed in table 2. These results give an accurate estimation of the variation of T_N with concentration, allowing the formation of a phase diagram (figure 7) when combined with the T_{sp}-measurements discussed previously. In figure 7, P = paramagnetic (1D antiferromagnetic), SP = the spin–Peierls state and AF = the Néel state observed in doped crystals. The crosses come from susceptibility measurements on Zn-doped polycrystalline samples made by Hase *et al* [1] and are included for comparison.

Now taking a closer look at a crystal of $CuGeO_3$ doped with 2.4% Zn, we extended our previous work on this sample [16] and performed elastic neutron scattering at the $(0, 1, 1/2)$ peak over the temperature range 0.3 K to 5 K (figure 8). Hase *et al* [15] recently took measurements on a 3.4% Zn-doped crystal that has the same T_N as our 2.4% Zn-doped

Table 2. Critical exponents for doped derivatives of $CuGeO_3$. T_{sp} and β are obtained from power law fitting to the order parameters at $\boldsymbol{Q} = (1/2, 3, 1/2)$, using the equation : $I = I_0(1-T/T_{sp})^{\beta}$. Some of these curves are shown in figure 6. T_N is obtained from straight line fits to the order parameter measured at $\boldsymbol{Q} = (0, 1, 1/2)$.

	Crystal	T_{sp} (K)	β (approx)	T_N (K) (approx)
Pure	$CuGeO_3$	14.04 ± 0.04	0.3(1)	0
Zn-doped	1.2	12.2 ± 0.1	0.3(3)	2.3
(%)	1.5	12.06 ± 0.05	0.3(7)	2.4
	2.0	11.6 ± 0.1	0.4(7)	4.0
	2.4	11.6 ± 0.1	0.5(0)	4.4
Ni-doped	1.7	11.53 ± 0.02	0.4(3)	2.3
(%)	1.9	11.50 ± 0.01	0.4(5)	2.5
	2.9	9.17* ± 0.07	0.4(4)	2.6
	3.3	Not observed	—	4.2(6)
	6.0	Not observed	—	3.2(0)

* Obtained from x-ray scattering on a small portion of crystal [35].

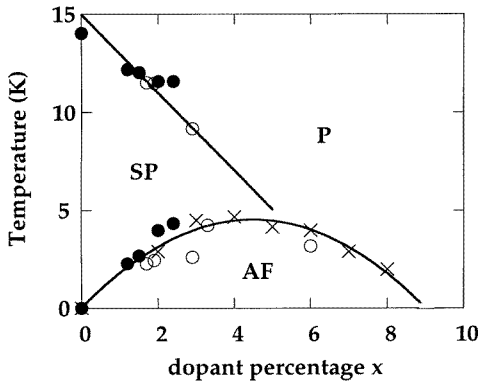

Figure 7. The phase diagram for Zn- (filled circles) and Ni- (open circles) doped $CuGeO_3$. The crosses correspond to susceptibility measurements on a series of Zn-doped crystals made by Hase *et al* [12].

crystal. They measured for temperatures $\geqslant$1.4 K and therefore failed to observe saturation of the moment. We extended our measurements to 0.3 K using a ^{3}He refrigerator and observed the onset of saturation of the magnetic moment which is apparent from the sharp change in gradient at 1.5 K. In the light of our evidence, the estimation given by Hase *et al* of the magnetic moment μ_{eff} = 0.19 μ_B at 2.2 K, must be scaled upwards to estimate a value of the saturated moment at 0.5 K. We obtain μ_{eff} = 0.24 μ_B at 0.5 K. This value is still much smaller than typical values for the Cu^{2+} ion in compounds such as $KCuF_3$ [30] (0.49 μ_B).

We have also used neutron scattering to investigate the direction of the magnetic moments in the low-temperature antiferromagnetic state for a range of doped crystals, by taking measurements at $\boldsymbol{Q} = (0, 1, 1/2)$, $(0, 3, 1/2)$, $(0, 3, 3/2)$ and $(0, 1, 3/2)$ at two temperatures—one scan below and one scan above T_N. Characteristic plots are shown in figure 9 for crystals doped with 2.4% Zn and 2.9% Ni to give an indication of the variation of peak intensity with position in reciprocal space and temperature. The anisotropy in figure 9 suggests that the antiferromagnetic structure can be described using a simple collinear model.

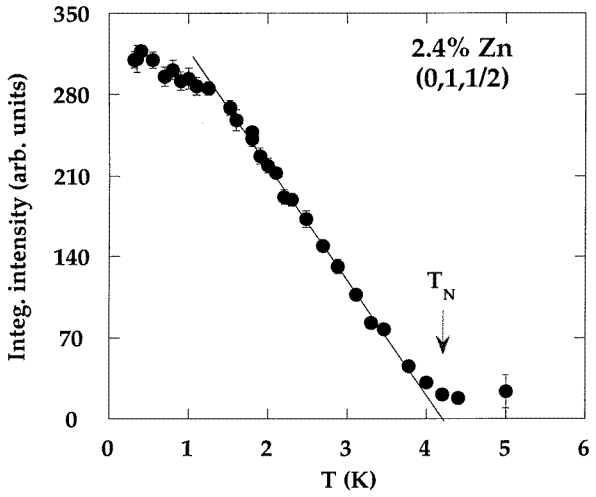

Figure 8. The temperature dependence of the peak at the superlattice magnetic reflection $\boldsymbol{Q} = (0, 1, 1/2)$ for the 2.4% Zn-doped $CuGeO_3$ crystal. Note the change of slope at 1.5 K and the linear behaviour of the order parameter from 1.5 K to 4 K.

In general, the integrated neutron scattering intensity of a magnetic peak can be written as

$$\frac{I^m_{hkl}}{I^n_{001}} = \frac{(M^{\perp}_{hkl})^2 (F^m_{hkl})^2 L(2\Theta_{hkl})}{(F_{001})^2 L(2\Theta_{001})}. \tag{2}$$

Here $F^m_{hkl} = 2f(Q)$ is the magnetic structure amplitude for each of the scattering $\boldsymbol{Q}$-vectors for the (h, k, l) magnetic Bragg reflections considered and $f(Q)$ is the Cu^{2+} form factor [31] at that position; the coefficient of $f(Q)$ is a geometrical structure factor,

$$(1 - e^{2\pi i(h+k+l)}) \tag{3}$$

which is 2 for every magnetic reflection that we observed. $L(2\Theta)$ is the Lorentz factor which can be written as $1/\sin(2\Theta)$. The selection rule for the magnetic scattering is included in $M^{\perp}_{hkl}$—the component of the moment perpendicular to the scattering vector, from which the magnetic moment in each crystal can be deduced. Assuming a random orientation of the unitary spin direction, $\hat{\boldsymbol{s}} = (s_x, s_y, s_z)$ and for a vector $\hat{\boldsymbol{Q}}$ oriented in the b^*–c^* plane, $\hat{\boldsymbol{Q}} = (0, \sin\alpha, \cos\alpha)$, where the angle α describes the rotation of the $\boldsymbol{Q}$-vector from the c^*-axis (see figures 10, left), we get (in an unsimplified form)

$$\begin{aligned} M^{\perp}_{hkl} &\equiv \hat{\boldsymbol{Q}} \times (\hat{\boldsymbol{s}} \times \hat{\boldsymbol{Q}}) \\ &= \hat{\boldsymbol{a}}(s_x) + \hat{\boldsymbol{b}}(s_y \cos^2(\alpha) - s_z \sin(\alpha)\cos(\alpha)) + \hat{\boldsymbol{c}}(s_z \sin^2(\alpha) - s_y \sin(\alpha)\cos(\alpha)). \end{aligned} \tag{4}$$

Values of $M^{\perp}_{hkl}$ calculated for four crystals, using equation (2) with I^n_{001} set to 1, are plotted versus α in figure 10 (right) with curves fitted from equation (4). Given that the magnitude of $M^{\perp}_{hkl}$ will be largest when $\hat{\boldsymbol{Q}}$ is perpendicular to the magnetic moment and using equation (4), we deduce that the Zn^{2+}-doped crystals have a moment almost completely along the c^*-axis. For the Ni^{2+}-doped crystals there is little variation in $M^{\perp}_{hkl}$ as α increases. This suggests that the moments in these crystals are aligned along the a^*-direction (and therefore are always $\perp$ to $\hat{\boldsymbol{Q}}$) with only a small component in the b^*- or c^*-directions, within experimental accuracy.

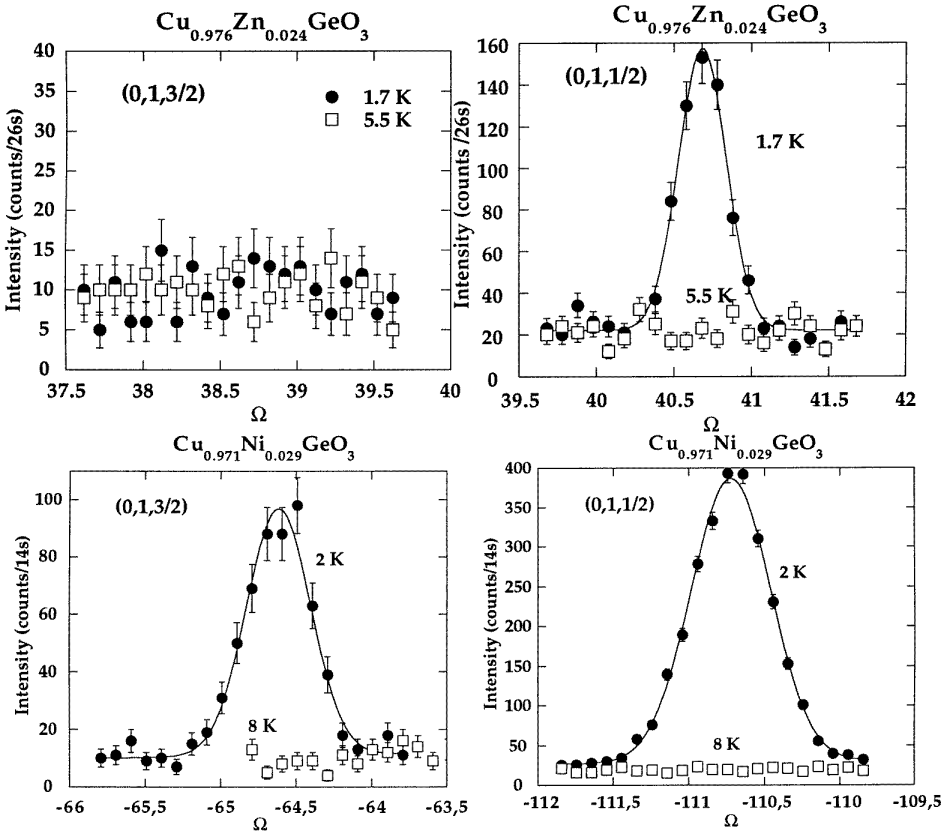

Figure 9. A comparison of neutron diffraction spectra at two magnetic wavevectors: $\boldsymbol{Q} = (0, 1, 3/2)$ (left) and $\boldsymbol{Q} = (0, 1, 1/2)$ (right) for a $Cu_{0.976}Zn_{0.024}GeO_3$ single crystal at 1.7 K and 5.5 K, and a $Cu_{0.971}Ni_{0.029}GeO_3$ single crystal at 2 K and 8 K.

4. Discussion

From the evidence presented above, we can conclude that the main effects of the presence of impurities in the S–P system $CuGeO_3$ are to suppress the transition temperature T_{sp} and lead to the emergence of a long-range Néel state at low temperatures. However, actual microscopic models of the role of impurities have not yet been developed, partly due to the departures of $CuGeO_3$ from ideal S–P behaviour. It seems reasonable, however, to surmise that a small amount of dopant acts to disturb the chains of Cu^{2+} ions, destroying long-range S–P order and simultaneously increasing the importance of 3D interactions between the magnetic moments. A mean-field approach to a valence bond solid [26] uses the starting assumption that the correlations along the chains are randomly interrupted by impurity ions to predict that in doped crystals, T_{sp} will be proportional to $(1 - x)$ where x is the dopant concentration. In figure 7 this linear behaviour is reproduced. Compare this graph to figure 11 where the integrated intensity of the superlattice peak at $(1/2, 3, 1/2)$ at 5 K is plotted versus dopant percentage. Clearly T_{sp} does not change significantly with dopant concentration, while the intensity of the reflection rapidly diminishes as x increases. As the intensity of a superlattice peak $I \propto \delta^2$, where δ is the displacement of the atoms in

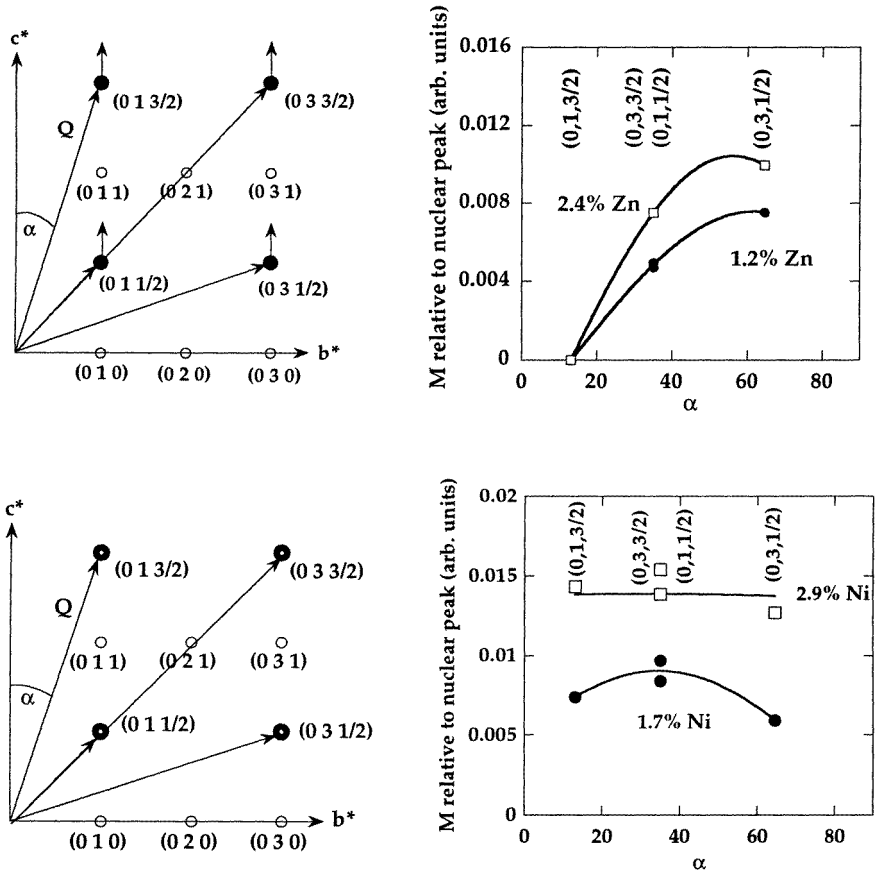

Figure 10. Schematic diagrams relating the scattering vectors for four antiferromagnetic reflections to the direction of the magnetic moments for (top left) Zn-doped crystals ($\mu \parallel c$) and (bottom left) Ni-doped crystals ($\mu \parallel a$). The $M_{hkl}^{\perp}$ versus α for these reflections, fitted with the curve derived from equation (4), are shown on the right, top and bottom.

the dimerized system [23], it seems that the effect of increased doping is either to lower the value of δ or to decrease the volume of the dimerized regions within the S–P crystal. If the latter interpretation is correct, the doped crystal can be visualized as comprised of S–P regions separated by impurities. The average volume of these regions decreases as x increases.

An additional effect of doping into $CuGeO_3$ is the appearance of a low-temperature 3D antiferromagnetic state. Again, from the phase diagram in figure 7 for low levels of dopant ions, T_N increases with concentration, to a maximum at $x = 4\%$, then decreases until at the highest concentration measured—6% Ni—T_N is now only 3.2 K. It is postulated by Hase *et al* [15] for $Cu_{1-x}Zn_xGeO_3$ and Renard *et al* [13] for $CuGe_{1-x}Si_xO_3$ that at small concentrations the impurities break up the linear Cu^{2+} chains, disrupting S–P correlations along the chains and allowing the fragmented portions to have increased interchain interactions, which ultimately leads to long-range 3D AF order. A different perspective comes from the work of Dupas and Renard [32] A quasi-1D antiferromagnet

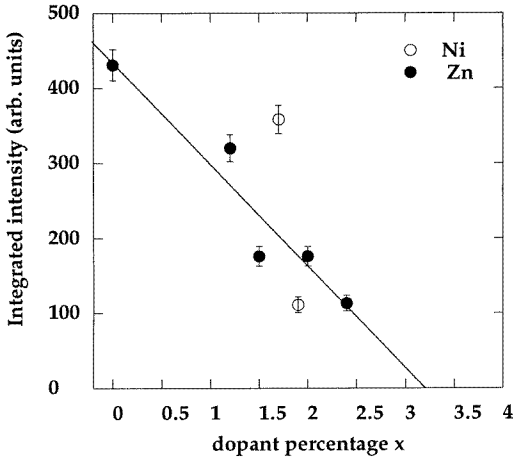

Figure 11. The integrated intensity of the $(1/2, 3, 1/2)$ superlattice peak at 5 K normalized to the sample volume versus dopant concentration for Ni- and Zn-doped crystals of $CuGeO_3$. The line is a guide to the eye.

with a gap is prevented from achieving long-range 3D order because the 1D spin-correlation length, ζ, tends to a constant value as $T \to 0$,

$$\zeta \propto J/\Delta \tag{5}$$

(where J is the interchain exchange coefficient), instead of diverging as is the case for a gapless quasi-1D antiferromagnet. Doping into this system reduces Δ, allowing ζ to increase and then diverge at low temperatures as $\Delta \to 0$. Renard *et al* use this argument to postulate that the energy gap disappears for a dopant concentration that corresponds to the maximum T_N, for our results, at $x = 4\%$. We have performed some inelastic neutron measurements on a 2.4% Zn-doped crystal and found no sign of an energy gap, although there is evidence that dimerization does occur, as can be seen from the weak superlattice reflection at $\boldsymbol{Q} = (1/2, 3, 1/2)$ in figure 6 as well as the small minimum in the susceptibility data at approximately 10 K in figure 4. The existence of a gapless S–P state in doped $CuGeO_3$ was first suggested by Blinc *et al* [33] and we plan further investigations of this phenomenon. The decrease in T_N as the dopant concentration is increased past the optimum level can be explained as due to the increasing hindrance of the AF correlations between Cu^{2+} chains. The correlation length decreases and so does T_N.

Taking a look at the correlation lengths along k and l in real space for the $(0, 1, 1/2)$ magnetic peak in the 2.4% Zn-doped crystal, and comparing them to the $(0, 0, 1)$ nuclear peak via the equation below, assuming a gaussian lineshape convoluted with a gaussian resolution function,

$$\Delta c = \sqrt{\mathrm{FWHM}^2_{(0,1,1/2)} - \mathrm{FWHM}^2_{(0,0,1)}} \tag{6}$$

gives, for the l-scans at 0.55 K, $\Delta c_l = 185$ Å, while the k-scans taken at 0.70 K gave $\Delta c_k = 623$ Å. Therefore in real space the magnetic correlation length is a lot larger in the k-direction than in the l-scan where it closely matches the correlations of the nuclear Bragg peaks.

5. Conclusion

We have presented results from susceptibility and neutron scattering measurements on a range of Ni^{2+}- and Zn^{2+}-doped single crystals of $CuGeO_3$ with concentrations from 0.5% to 6%. We have found that doping with Zn or Ni suppresses the S–P state and leads to the emergence of long-range Néel order at low temperatures, in broad agreement with the work of Hase *et al*. A new result is the extension of measurements on a 2.4% Zn-doped crystal to temperatures below 1.5 K where a change of slope in the intensity of the $(0, 1, 1/2)$ magnetic peak indicates the onset of saturation of the moment. The current picture of doped $CuGeO_3$ is that the impurities probably act to divide the 1D AF chains into smaller sections of spin–Peierls material that interact via an enhanced superexchange mechanism. Our measurements of T_N versus x show that T_N is suppressed for dopant concentrations $>4\%$, in support of the idea that beyond a certain concentration of impurities, interchain interactions are hindered and cannot propagate in three dimensions. In order to determine the direction of the magnetic moment in the Néel state for the Ni- and Zn-doped crystals, we have measured the intensity of the magnetic reflections $(0, 1, 1/2)$, $(0, 3, 1/2)$, $(0, 1, 3/2)$ and $(0, 3, 3/2)$. Our results show that for the Zn^{2+}-doped crystals the magnetic moment is still aligned in the c^*-direction but below T_N in the Ni-doped crystals the moment now aligns primarily in the a^*-direction. This situation is analogous to the 2D compound La_2CuO_4 when some Cu^{2+} ions are replaced by either Zn^{2+} or Ni^{2+} [34]. Pogorel'tsev *et al* have found that doping with non-magnetic Zn does not change the magnetic order while doping with magnetic Ni produces a change in the orientation of the magnetic moment. It is assumed that the Ni impurity perturbs the nearest-neighbour spin environment in the Cu–O planes which becomes significant for concentrations $\geqslant 5\%$. For a lower-dimensional compound like $Cu_{1-x}Ni_xGeO_3$, we expect the effect of doping with magnetic impurities to be correspondingly greater.

Acknowledgments

We would like to acknowledge the Chemistry Departments at Risø and the University of Warwick for performing spectroscopy measurements on our crystals. The Interdisciplinary Research Centre at Cambridge was extremely helpful in providing time on their SQUID. Financial support for the work at Risø came from the Large Scale Facility Programme of the EC and the work in Warwick was funded by the EPSRC.

References

[1] Hase M, Terasaki I and Uchinokura K 1993 *Phys. Rev. Lett.* **70** 3651
[2] Haldane F D 1983 *Phys. Lett.* **93A** 464
[3] Haldane F D 1983 *Phys. Rev. Lett.* **50** 1153
[4] Nishi M, Fujita O and Akimitsu K 1994 *Phys. Rev.* B **50** 6508
[5] Lussier J-G, Coad S, McMorrow D F and Paul D McK 1996 *J. Phys.: Condens. Matter* **8** L59
[6] Fujita O, Akimitsu T, Nishi M and Kakurai K 1995 *Phys. Rev. Lett.* **74** 1677
[7] Hirota K, Cox D, Lorenzo J, Shirane G, Tranquada J, Hase M, Uchinokura K, Kojima H, Shibuya Y and Tanaka I 1994 *Phys. Rev. Lett.* **73** 786
[8] Jacobs I, Bray J, Hart H, Interrante L, Kasper J, Watkins G, Prober D and Bonner J 1976 *Phys. Rev.* B **14** 3036
[9] Bray J, Hart H, Interrante L, Jacobs I, Kasper J, Watkins G, Wee S and Bonner J 1975 *Phys. Rev. Lett.* **35** 744
[10] Moncton D, Birgeneau R, Interrante L and Wudl F 1977 *Phys. Rev. Lett.* **39** 507

[11] Tchernyshov O, Blaer A S, Keren A, Kojima K, Luke G M, Wu W D, Uemura Y J, Hase M, Uchinokura K, Ajiro Y, Asano T and Mekata M 1995 *J. Magn. Magn. Mater.* **140–144** 1687
[12] Hase M, Terasaki I, Sasago Y, Uchinokura K and Obara H 1994 *Physica* B **194** 269
[13] Renard J-P, Le Dang K, Veillet P, Dhalenne G, Revcolevschi A and Regnault L-P 1995 *Europhys. Lett.* **30** 475
[14] Regnault L P, Ain M, Hennion B, Dhalenne G and Revcolevschi A 1995 *Physica* B **213, 214** 278
[15] Hase M, Uchinokura K, Birgeneau R, Hirota K and Shirane G 1996 *J. Phys. Soc. Japan* **65** 273
[16] Lussier J-G, Coad S, McMorrow D F and Paul D McK 1995 *J. Phys.: Condens. Matter* **7** L325
Note that the temperatures in the text are not those of figure 3. For the Zn-doped compound we found $T_N = 4.2$ K and for the Ni-doped compound, $T_N = 2.8$ K.
[17] Hase M, Terasaki I, Sasago Y, Uchinokura K and Obara H 1993 *Phys. Rev. Lett.* **71** 4059
[18] Bonner J and Fisher M 1964 *Phys. Rev.* A **135** 640
[19] Bonner J and Blote H 1982 *Phys. Rev.* B **25** 6959
[20] Bulaevskii L 1969 *Sov. Phys.–Solid State* **11** 921
[21] des Cloiseaux J and Pearson J 1962 *Phys. Rev.* **128** 2131
[22] Nojiri H, Shimamoto Y, Miura N, Hase M, Uchinokura K, Kojima H, Tanaka I and Shibuya Y 1995 *Phys. Rev.* B **52** 12 749
[23] Riera J and Dobry A 1995 *Phys. Rev.* B **51** 16 098
[24] Castilla G, Chakravarty S and Emery V J 1995 *Phys. Rev. Lett.* **75** 1823
[25] Cowley R A, Lake B and Tennant D A 1996 *J. Phys.: Condens. Matter* **8** L179
[26] Lu Z-Y, Su Z-B and Yu L 1994 *Phys. Rev. Lett.* **72** 1276
[27] Liu Y, Drumheller J and Willett R 1995 *Phys. Rev.* B **52** 15 327
[28] Ajiro Y, Asano T, Masui F, Mekata M, Aruga-Katori H, Goto T and Kikuchi H 1995 *Phys. Rev.* B **51** 9399
[29] Collins M F 1989 *Magnetic Critical Scattering* (Oxford: Oxford University Press)
[30] Hutchings M, Samuelson E, Shirane G and Hirakawa K 1969 *Phys. Rev.* B **188** 919
[31] *International Tables for Crystallography* 1993 (Dordrecht: Kluwer Academic)
[32] Dupas C and Renard J-P 1978 *Phys. Rev.* B **18** 401
[33] Blinc R, Cevc P, Arcon D, Lappas A, Prassides K and Volkel G 1995 *Solid State Commun.* **94** 593
[34] Pogorel'tsev A, Matukhin V, Anashkin V, Safin I, Matukhina L and Kukovitskii E 1995 *JETP Lett.* **62** 568
[35] Kiryukhin V, Keimer B, Hill J, Coad S and Paul D 1996 *Phys. Rev.* B at press